GEOPHYSICS, VOL. 82, NO. 3 (MAY-JUNE 2017); P. T121–T132, 6 FIGS., 5 TABLES.
10.1190/GEO2016-0457.1

A general optimal method for a 2D frequency-domain finite-difference solution of scalar wave equation

Na Fan[1], Lian-Feng Zhao[2], Xiao-Bi Xie[3], Xin-Gong Tang[1], and Zhen-Xing Yao[2]

ABSTRACT

We have developed a general optimal method for 2D frequency-domain finite-difference simulation of the scalar wave equation. For a given finite-difference stencil, this method can generate the dispersion equation and optimize the expansion coefficients. Many commonly used frequency-domain finite-difference schemes (e.g., grids with different numbers of points, rotated grids, and grid spaces with different aspect ratios) can be derived as special cases under this framework. The possibility of expanding this method to 3D does exist. Based on the 2D scalar wave equation, the optimized coefficients of 25-point, 9-point, 17-point, and 15-point schemes have been worked out. The dispersion analysis indicates that our 25-point scheme has much higher accuracy than the average-derivative method 25-point scheme. The number of grid points per the smallest wavelength is reduced from 2.78 to 2.13 for a maximum phase velocity errors of 1%. The synthetic seismograms and the wavefield snapshots calculated using our optimal 25-point finite-different scheme give smaller dispersions than other finite-difference schemes.

INTRODUCTION

The frequency-domain finite-difference (FD) method plays an important role in seismic forward modeling and frequency-domain full-waveform inversion (FWI), in which, due to multiple iterations, tremendous computation costs are involved in FD calculations (Pratt, 1999; Brossier et al., 2009; Virieux and Operto, 2009). Therefore, increasing the accuracy and efficiency of frequency-domain forward modeling attracted much attention. The accuracy of an FD operator can be affected by expansion coefficients. Using optimized coefficients can effectively reduce numerical dispersions and reduce the required number of grid points per wavelength. This can largely reduce the effort in solving the matrix inversion and speed up FD calculation. Pratt and Worthington (1990) develop the classic five-point FD operator for the frequency-domain 2D scalar wave equation, and it needs 13 grid points per wavelength to lower the phase velocity errors to below 1%. To reduce G (number of grid points per wavelength required in numerical calculations), the rotating coordinate system has been widely used (Jo et al., 1996; Shin and Sohn, 1998; Štekl and Pratt, 1998; Hustedt et al., 2004; Operto et al., 2007, 2009, 2014; Cao and Chen, 2012).

Using conventional 0° and 45° FD operators to approximate the Laplacian and mass acceleration terms, Jo et al. (1996) develop an optimal nine-point operator for the scalar wave equation and reduce G to approximately four. Later, by combining FD operators of 0°, 26.6°, 45°, and 63.4°, Shin and Sohn (1998) develop an optimal 25-point operator and reduce G to 2.5. Cao and Chen (2012) combine 0° and 45° FD operators to form an optimal 17-point scheme that needs 2.56 grid points per wavelength. However, the rotated optimal schemes require the same spatial sampling intervals in the x- and z-directions, which limited their applications in practice. Targeted to the rectangular grid, Chen (2012) proposes a new optimal nine-point scheme based on the average-derivative method (ADM). This algorithm actually includes Jo's rotated nine-point scheme as a special case. Later, Zhang et al. (2014, 2015) propose the ADM 25-point scheme that includes the rotated 25-point scheme of Shin and Sohn (1998) as a special case. Tang et al. (2015) propose the ADM 17-point scheme that also includes the rotated 17-point scheme of Cao and Chen (2012) as a special case. Because these rotated optimal schemes are all special cases of the corresponding optimal ADM schemes, the latter should be equally accurate to or more accurate than the former. In addition to the commonly used 9-, 25-, and 17-point schemes, Liu et al. (2013) propose a 15-point

Manuscript received by the Editor 30 August 2016; revised manuscript received 7 January 2017; published online 10 April 2017.
[1]Yangtze University, School of Geophysics and Oil Resources and Key Laboratory of Exploration Technologies for Oil and Gas Resources, Ministry of Education, Wuhan, China. E-mail: fannachina@hotmail.com; tangxg@yangtzeu.edu.cn.
[2]Chinese Academy of Sciences, Institute of Geology and Geophysics, Key Laboratory of Earth and Planetary Physics, Beijing, China. E-mail: zhaolf@mail.iggcas.ac.cn; yaozx@mail.iggcas.ac.cn.
[3]University of California at Santa Cruz, Institute of Geophysics and Planetary Physics, Santa Cruz, California, USA. E-mail: xxie@ucsc.edu.

scheme aimed at effectively suppressing dispersions with smaller bandwidth in the impedance matrix. Although only equal intervals were considered, this method can also be applied to the rectangular grid. Those different optimal schemes for the 2D scalar wave equation have been widely used and expanded to 3D, elastic, and anisotropic cases (Operto et al., 2009, 2014; Chen, 2014; Li et al., 2015; Chen and Cao, 2016).

There usually exists a general optimal method to determine the coefficients of an FD operator with different stencils for time-domain FD modeling (Holberg, 1987; Liu and Sen, 2009; Zhang and Yao, 2013). However, for frequency-domain FD methods, unlike their time-domain counterparts, different schemes, e.g., 25-, 9-, 17-, and 15-point schemes, usually have their own forms of differential equations with different distributions of optimized coefficients. In this paper, we propose a general optimal method for frequency-domain FD modeling based on 2D scalar wave equation. This paper is organized as follows. First, we illustrate the theory of our method. Then, we give the numerical experiments to demonstrate the theoretical analysis, and finally we state our conclusions.

THEORY

A general finite-difference scheme

The 2D scalar wave (constant-density acoustic wave) equation in the frequency domain is given by

$$\frac{\partial^2 P}{\partial x^2}+\frac{\partial^2 P}{\partial z^2}+\frac{\omega^2}{v^2}P=0, \tag{1}$$

where P is the pressure wavefield, ω is the angular frequency, and v is the velocity. Assuming that the wavefield values of several neighboring points all contribute to the approximations of spatial derivatives $\partial^2 P/\partial x^2$ and $\partial^2 P/\partial z^2$ of the central point, and the contribution weights of the neighboring points are identical if the distance from the neighboring points to the central point is equal. To our knowledge, 25 are the most points involved in a frequency-domain FD operator. Therefore, we introduce a general 25-point scheme (Figure 1a) to approximate the spatial derivatives:

$$\begin{aligned}\frac{\partial^2 P}{\partial x^2}\approx\frac{1}{\Delta x^2}[&c_0P_{m,n}+c_1(P_{m-1,n}+P_{m+1,n})+c_2(P_{m,n-1}+P_{m,n+1})\\&+c_3(P_{m-1,n-1}+P_{m+1,n+1}+P_{m-1,n+1}+P_{m+1,n-1})\\&+c_4(P_{m-2,n}+P_{m+2,n})+c_5(P_{m,n-2}+P_{m,n+2})\\&+c_6(P_{m-2,n-1}+P_{m+2,n+1}+P_{m+2,n-1}+P_{m-2,n+1})\\&+c_7(P_{m-1,n-2}+P_{m+1,n+2}+P_{m-1,n+2}+P_{m+1,n-2})\\&+c_8(P_{m-2,n-2}+P_{m+2,n+2}+P_{m-2,n+2}+P_{m+2,n-2})],\end{aligned} \tag{2a}$$

$$\begin{aligned}\frac{\partial^2 P}{\partial z^2}\approx\frac{1}{\Delta z^2}[&d_0P_{m,n}+d_1(P_{m-1,n}+P_{m+1,n})+d_2(P_{m,n-1}+P_{m,n+1})\\&+d_3(P_{m-1,n-1}+P_{m+1,n+1}+P_{m-1,n+1}+P_{m+1,n-1})\\&+d_4(P_{m-2,n}+P_{m+2,n})+d_5(P_{m,n-2}+P_{m,n+2})\\&+d_6(P_{m-2,n-1}+P_{m+2,n+1}+P_{m+2,n-1}+P_{m-2,n+1})\\&+d_7(P_{m-1,n-2}+P_{m+1,n+2}+P_{m-1,n+2}+P_{m+1,n-2})\\&+d_8(P_{m-2,n-2}+P_{m+2,n+2}+P_{m-2,n+2}+P_{m+2,n-2})],\end{aligned} \tag{2b}$$

where $P_{m,n}=P(m\Delta x,n\Delta z)$, Δx, and Δz are the spatial sampling intervals in the x- and z-directions, c_i are the weighting coefficients to approximate $\partial^2 P/\partial x^2$, and subscript i identifies locations shown in Figure 1a. Converting equation 2a into the wavenumber domain and let $k=0$, then c_i satisfy the following relationship:

$$c_0+2c_1+2c_2+4c_3+2c_4+2c_5+4c_6+4c_7+4c_8=0. \tag{3}$$

Similarly, d_i are the weighting coefficients to approximate $\partial^2 P/\partial z^2$ and satisfy

$$d_0+2d_1+2d_2+4d_3+2d_4+2d_5+4d_6+4d_7+4d_8=0. \tag{4}$$

The mass acceleration term $(\omega^2/v^2)P$ is approximated by linearly combining the wavefield at 25 neighboring points. Substituting these terms into equation 1, we obtain the following scheme:

$$\begin{aligned}\frac{1}{\Delta x^2}[&c_0P_{m,n}+c_1(P_{m-1,n}+P_{m+1,n})+c_2(P_{m,n-1}+P_{m,n+1})\\&+c_3(P_{m-1,n-1}+P_{m+1,n+1}+P_{m-1,n+1}+P_{m+1,n-1})\\&+c_4(P_{m-2,n}+P_{m+2,n})+c_5(P_{m,n-2}+P_{m,n+2})\\&+c_6(P_{m-2,n-1}+P_{m+2,n+1}+P_{m+2,n-1}+P_{m-2,n+1})\\&+c_7(P_{m-1,n-2}+P_{m+1,n+2}+P_{m-1,n+2}+P_{m+1,n-2})\\&+c_8(P_{m-2,n-2}+P_{m+2,n+2}+P_{m-2,n+2}+P_{m+2,n-2})]\end{aligned}$$

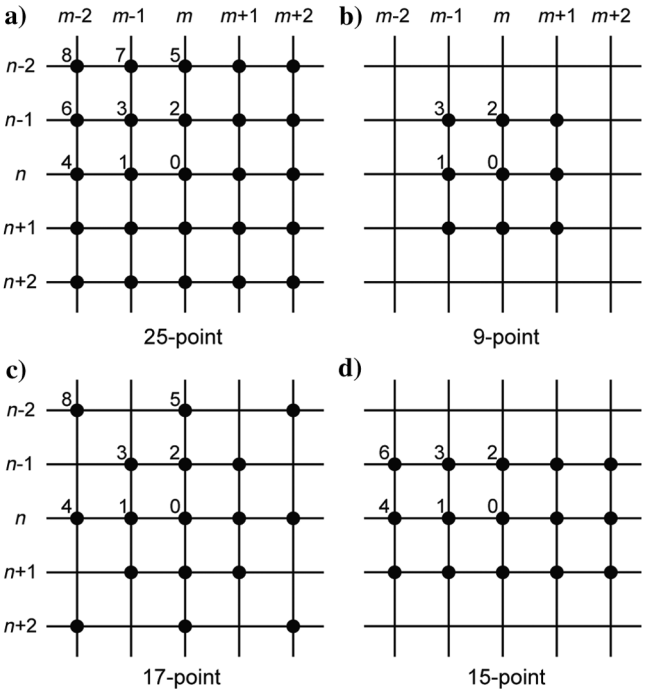

Figure 1. Grid configurations for different 2D frequency-domain FD operators, with the (a) 25-point scheme, (b) 9-point scheme, (c) 17-point scheme, and (d) 15-point scheme.

$$+\frac{1}{\Delta z^2}[d_0P_{m,n}+d_1(P_{m-1,n}+P_{m+1,n})+d_2(P_{m,n-1}+P_{m,n+1})$$
$$+d_3(P_{m-1,n-1}+P_{m+1,n+1}+P_{m-1,n+1}+P_{m+1,n-1})$$
$$+d_4(P_{m-2,n}+P_{m+2,n})+d_5(P_{m,n-2}+P_{m,n+2})$$
$$+d_6(P_{m-2,n-1}+P_{m+2,n+1}+P_{m+2,n-1}+P_{m-2,n+1})$$
$$+d_7(P_{m-1,n-2}+P_{m+1,n+2}+P_{m-1,n+2}+P_{m+1,n-2})$$
$$+d_8(P_{m-2,n-2}+P_{m+2,n+2}+P_{m-2,n+2}+P_{m+2,n-2})]$$
$$+\frac{\omega^2}{v^2}[b_0P_{m,n}+b_1(P_{m-1,n}+P_{m+1,n})+b_2(P_{m,n-1}+P_{m,n+1})$$
$$+b_3(P_{m-1,n-1}+P_{m+1,n+1}+P_{m-1,n+1}+P_{m+1,n-1})$$
$$+b_4(P_{m-2,n}+P_{m+2,n})+b_5(P_{m,n-2}+P_{m,n+2})$$
$$+b_6(P_{m-2,n-1}+P_{m+2,n+1}+P_{m+2,n-1}+P_{m-2,n+1})$$
$$+b_7(P_{m-1,n-2}+P_{m+1,n+2}+P_{m-1,n+2}+P_{m+1,n-2})$$
$$+b_8(P_{m-2,n-2}+P_{m+2,n+2}+P_{m-2,n+2}+P_{m+2,n-2})]=0, \quad (5)$$

where b_i are the weighting coefficients of the mass acceleration term and satisfy

$$b_0+2b_1+2b_2+4b_3+2b_4+2b_5+4b_6+4b_7+4b_8=1. \quad (6)$$

The scheme described in equation 5 actually includes the classic 5-point, classic 9-point, rotated 9-point (Jo et al., 1996), rotated 25-point (Shin and Sohn, 1998), rotated 17-point (Cao and Chen, 2012), ADM 9-point (Chen, 2012), ADM 25-point (Zhang et al., 2015), ADM 17-point (Tang et al., 2015), and 15-point (Liu et al., 2013) schemes as its special cases (refer to Figure 1 and Appendix A).

We first consider the case $\Delta x \geq \Delta z$. Substituting $r = \Delta x/\Delta z$ into equation 5 to eliminate Δz, and let

$$a_i = c_i + r^2 d_i \quad (i = 0, 1, 2, \ldots, 8). \quad (7)$$

By combining similar terms, we have

$$\frac{1}{\Delta x^2}[a_0P_{m,n}+a_1(P_{m-1,n}+P_{m+1,n})+a_2(P_{m,n-1}+P_{m,n+1})$$
$$+a_3(P_{m-1,n-1}+P_{m+1,n+1}+P_{m-1,n+1}+P_{m+1,n-1})$$
$$+a_4(P_{m-2,n}+P_{m+2,n})+a_5(P_{m,n-2}+P_{m,n+2})$$
$$+a_6(P_{m-2,n-1}+P_{m+2,n+1}+P_{m+2,n-1}+P_{m-2,n+1})$$
$$+a_7(P_{m-1,n-2}+P_{m+1,n+2}+P_{m-1,n+2}+P_{m+1,n-2})$$
$$+a_8(P_{m-2,n-2}+P_{m+2,n+2}+P_{m-2,n+2}+P_{m+2,n-2})]$$
$$+\frac{\omega^2}{v^2}[b_0P_{m,n}+b_1(P_{m-1,n}+P_{m+1,n})+b_2(P_{m,n-1}+P_{m,n+1})$$
$$+b_3(P_{m-1,n-1}+P_{m+1,n+1}+P_{m-1,n+1}+P_{m+1,n-1})$$
$$+b_4(P_{m-2,n}+P_{m+2,n})+b_5(P_{m,n-2}+P_{m,n+2})$$
$$+b_6(P_{m-2,n-1}+P_{m+2,n+1}+P_{m+2,n-1}+P_{m-2,n+1})$$
$$+b_7(P_{m-1,n-2}+P_{m+1,n+2}+P_{m-1,n+2}+P_{m+1,n-2})$$
$$+b_8(P_{m-2,n-2}+P_{m+2,n+2}+P_{m-2,n+2}+P_{m+2,n-2})]=0, \quad (8)$$

where, due to equations 3 and 4, a_i also satisfy the following relationship:

$$a_0 + 2a_1 + 2a_2 + 4a_3 + 2a_4 + 2a_5 + 4a_6 + 4a_7 + 4a_8 = 0. \quad (9)$$

Finally, equation 8 is the 25-point scheme to be optimized, and it is composed of 16 independent coefficients.

Dispersion analysis

To perform the dispersion analysis, we substitute a plane wave $P(x, z, \omega) = P_0 e^{-i(k_x x + k_z z)}$ into equation 8. The normalized phase velocity is obtained as

$$\frac{V_{\mathrm{ph}}}{v} = \frac{G}{2\pi} \times \sqrt{-\frac{a_0+2a_1T_1+2a_2T_2+4a_3T_3+2a_4T_4+2a_5T_5+4a_6T_6+4a_7T_7+4a_8T_8}{b_0+2b_1T_1+2b_2T_2+4b_3T_3+2b_4T_4+2b_5T_5+4b_6T_6+4b_7T_7+4b_8T_8}}, \quad (10)$$

where V_{ph} is the phase velocity, $T_1 = \cos(2\pi \sin\theta/G)$, $T_2 = \cos(2\pi \cos\theta/rG)$, $T_3 = \cos(2\pi \sin\theta/G)\cos(2\pi \cos\theta/rG)$, $T_4 = \cos(4\pi \sin\theta/G)$, $T_5 = \cos(4\pi \cos\theta/rG)$, $T_6 = \cos(4\pi \sin\theta/G)\cos(2\pi \cos\theta/rG)$, $T_7 = \cos(2\pi \sin\theta/G)\cos(4\pi \cos\theta/rG)$, and $T_8 = \cos(4\pi \sin\theta/G)\cos(4\pi \cos\theta/rG)$. The number of grid points per wavelength G is defined with respect to the larger spatial sampling interval $\max(\Delta x, \Delta z)$. For $\Delta x \geq \Delta z$, $G = 2\pi/k\Delta x$, θ is the propagation angle from the z-axis and satisfies $k_x = k \cdot \sin\theta$ and $k_z = k \cdot \cos\theta$. The 16 independent coefficients a_i and b_i $(i = 1, 2, \ldots, 8)$ are determined by minimizing the phase error:

$$E(a_1, \ldots, a_8, b_1, \ldots, b_8) = \iint \left[1 - \frac{V_{\mathrm{ph}}}{v}\right]^2 d\tilde{k} d\theta, \quad (11)$$

where $\tilde{k} = 1/G$. The range of propagation angle θ is $[0, \pi/2]$, and the range of $\tilde{k}$ is usually determined by the size of the FD stencil.

Boundary conditions

The perfectly matched layer (PML) absorbing boundary condition has been widely used in finite-difference calculations of the time and frequency domains (Berenger, 1994; Hustedt et al., 2004; Operto et al., 2009; Zhang and Shen, 2010; Tang et al., 2015). We adopt this method for the frequency-domain 2D scalar wave equation, and the derivation is given in Appendix B. The PML absorbing condition is written as

$$\frac{1}{s_x^2}\frac{\partial^2 P}{\partial x^2} + \frac{1}{s_z^2}\frac{\partial^2 P}{\partial z^2} + \frac{\omega^2}{v^2}P = 0, \quad (12)$$

where $s_x = 1 - 2\pi a f(i/\omega)(x/L)^2$, $s_z = 1 - 2\pi a f(i/\omega)(z/L)^2$, and L denotes the width of the PML layers in the x- and z-directions. The term f is the dominant frequency of the source wavelet and a is 1.79 in this paper. The general 25-point scheme for equation 12 is

$$
\begin{aligned}
&\frac{1}{s_x^2}\times\frac{1}{\Delta x^2}[c_0P_{m,n}+c_1(P_{m-1,n}+P_{m+1,n})+c_2(P_{m,n-1}+P_{m,n+1})\\
&+c_3(P_{m-1,n-1}+P_{m+1,n+1}+P_{m-1,n+1}+P_{m+1,n-1})\\
&+c_4(P_{m-2,n}+P_{m+2,n})+c_5(P_{m,n-2}+P_{m,n+2})\\
&+c_6(P_{m-2,n-1}+P_{m+2,n+1}+P_{m+2,n-1}+P_{m-2,n+1})\\
&+c_7(P_{m-1,n-2}+P_{m+1,n+2}+P_{m-1,n+2}+P_{m+1,n-2})\\
&+c_8(P_{m-2,n-2}+P_{m+2,n+2}+P_{m-2,n+2}+P_{m+2,n-2})]\\
&+\frac{1}{s_z^2}\times\frac{1}{\Delta z^2}[d_0P_{m,n}+d_1(P_{m-1,n}+P_{m+1,n})+d_2(P_{m,n-1}+P_{m,n+1})\\
&+d_3(P_{m-1,n-1}+P_{m+1,n+1}+P_{m-1,n+1}+P_{m+1,n-1})\\
&+d_4(P_{m-2,n}+P_{m+2,n})+d_5(P_{m,n-2}+P_{m,n+2})\\
&+d_6(P_{m-2,n-1}+P_{m+2,n+1}+P_{m+2,n-1}+P_{m-2,n+1})\\
&+d_7(P_{m-1,n-2}+P_{m+1,n+2}+P_{m-1,n+2}+P_{m+1,n-2})\\
&+d_8(P_{m-2,n-2}+P_{m+2,n+2}+P_{m-2,n+2}+P_{m+2,n-2})]\\
&+\frac{\omega^2}{v^2}[b_0P_{m,n}+b_1(P_{m-1,n}+P_{m+1,n})+b_2(P_{m,n-1}+P_{m,n+1})\\
&+b_3(P_{m-1,n-1}+P_{m+1,n+1}+P_{m-1,n+1}+P_{m+1,n-1})\\
&+b_4(P_{m-2,n}+P_{m+2,n})+b_5(P_{m,n-2}+P_{m,n+2})\\
&+b_6(P_{m-2,n-1}+P_{m+2,n+1}+P_{m+2,n-1}+P_{m-2,n+1})\\
&+b_7(P_{m-1,n-2}+P_{m+1,n+2}+P_{m-1,n+2}+P_{m+1,n-2})\\
&+b_8(P_{m-2,n-2}+P_{m+2,n+2}+P_{m-2,n+2}+P_{m+2,n-2})]\\
&=0. \qquad (13)
\end{aligned}
$$

To create PML layers, the coefficients c_i and d_i in equation 13 are required. Although they satisfy equation 7, additional constraints are needed to find c_i and d_i. Wave equation 1 can be converted to the frequency-wavenumber domain:

$$-k_x^2-k_z^2+\frac{\omega^2}{v^2}=0. \qquad (14)$$

Meanwhile, equation 5 has the following dispersion relation:

$$
\begin{aligned}
&\frac{1}{\Delta x^2}\frac{c_0+2c_1T_1+2c_2T_2+4c_3T_3+2c_4T_4+2c_5T_5+4c_6T_6+4c_7T_7+4c_8T_8}{b_0+2b_1T_1+2b_2T_2+4b_3T_3+2b_4T_4+2b_5T_5+4b_6T_6+4b_7T_7+4b_8T_8}\\
&+\frac{1}{\Delta z^2}\frac{d_0+2d_1T_1+2d_2T_2+4d_3T_3+2d_4T_4+2d_5T_5+4d_6T_6+4d_7T_7+4d_8T_8}{b_0+2b_1T_1+2b_2T_2+4b_3T_3+2b_4T_4+2b_5T_5+4b_6T_6+4b_7T_7+4b_8T_8}+\frac{\omega^2}{v^2}=0. \qquad (15)
\end{aligned}
$$

Comparing equations 14 and 15, we have

Table 1. Optimized coefficients for 25-point scheme, with different r values and $\Delta x \geq \Delta z$.

r	1.0	1.5	2.0	2.5	3.0
c_1	1.070581409E-01	1.516312072E-01	1.178376630E-01	1.019999403E-01	−1.866269565E-01
c_2	−1.767576808E-01	−1.409931644E-01	−1.958614156E-01	−2.109967922E-01	−3.165533827E-01
c_3	4.256192769E-02	2.836735847E-02	5.682945750E-02	7.540881098E-02	3.204453793E-01
c_4	1.018284686E-01	1.078883550E-01	1.007925034E-01	1.215583963E-01	4.492955319E-01
c_5	−8.748787859E-03	5.452362404E-03	1.601985244E-02	2.876462821E-02	1.688622453E-01
c_6	4.563706346E-02	4.124272471E-02	3.787079146E-02	2.263666887E-02	−1.732977612E-01
c_7	3.123956737E-04	−8.012712086E-03	−1.949568923E-02	−2.915224592E-02	−1.314869962E-01
c_8	4.191263861E-03	5.641732977E-03	1.254643788E-02	1.717397941E-02	4.960200629E-02
d_1	−1.767572659E-01	−2.052013087E-01	−8.750611120E-02	−9.006467626E-02	−6.422968448E-01
d_2	1.070585592E-01	2.374081437E-01	1.196115019E-01	1.739112134E-01	1.141408211E+00
d_3	4.256158052E-02	6.115338025E-02	−1.729095759E-02	−1.566656148E-02	3.523121691E-01
d_4	−8.749075471E-03	−5.182553193E-03	8.459349411E-03	2.420860666E-03	−1.342252669E-02
d_5	1.018283031E-01	6.926171885E-02	9.871268740E-02	8.520551176E-02	−1.569649392E-01
d_6	3.126192770E-04	−1.818578493E-03	−1.091138226E-02	−6.716052626E-03	3.641142159E-03
d_7	4.563720401E-02	4.141503238E-02	6.102659937E-02	6.069437043E-02	−3.116555125E-02
d_8	4.191188409E-03	4.423206779E-03	6.687744857E-03	5.503423691E-03	3.071774803E-03
b_1	1.164330370E-01	1.253203454E-01	1.064415834E-01	1.114794218E-01	3.242659420E-01
b_2	1.164330350E-01	1.001495493E-01	1.263628490E-01	1.222668350E-01	2.573138391E-02
b_3	5.172956970E-02	4.748407064E-02	5.292261915E-02	4.980799522E-02	−6.237550759E-02
b_4	7.133814065E-03	4.928694220E-03	−2.758738099E-03	−2.645256080E-03	−4.057169514E-02
b_5	7.133775482E-03	2.351844201E-03	2.782337180E-03	5.557663865E-04	−3.696395730E-02
b_6	4.059695134E-03	5.384959483E-03	1.001719660E-02	1.000023201E-02	3.732229414E-02
b_7	4.059713283E-03	3.878802969E-03	7.868621831E-03	8.334418436E-03	1.431993964E-02
b_8	5.473012216E-06	−2.061596657E-04	−9.973342350E-04	−1.081750312E-03	−9.363613598E-03

$$-(k_x\Delta x)^2 \approx \frac{c_0+2c_1T_1+2c_2T_2+4c_3T_3+2c_4T_4+2c_5T_5+4c_6T_6+4c_7T_7+4c_8T_8}{b_0+2b_1T_1+2b_2T_2+4b_3T_3+2b_4T_4+2b_5T_5+4b_6T_6+4b_7T_7+4b_8T_8} \tag{16a}$$

and

$$-(k_z\Delta z)^2 \approx \frac{d_0+2d_1T_1+2d_2T_2+4d_3T_3+2d_4T_4+2d_5T_5+4d_6T_6+4d_7T_7+4d_8T_8}{b_0+2b_1T_1+2b_2T_2+4b_3T_3+2b_4T_4+2b_5T_5+4b_6T_6+4b_7T_7+4b_8T_8} \tag{16b}$$

By creating two functions,

$$E_1 = \frac{c_0+2c_1T_1+2c_2T_2+4c_3T_3+2c_4T_4+2c_5T_5+4c_6T_6+4c_7T_7+4c_8T_8}{b_0+2b_1T_1+2b_2T_2+4b_3T_3+2b_4T_4+2b_5T_5+4b_6T_6+4b_7T_7+4b_8T} + \left(\frac{2\pi\sin\theta}{G}\right)^2, \tag{17a}$$

and

$$E_2 = \frac{d_0+2d_1T_1+2d_2T_2+4d_3T_3+2d_4T_4+2d_5T_5+4d_6T_6+4d_7T_7+4d_8T_8}{b_0+2b_1T_1+2b_2T_2+4b_3T_3+2b_4T_4+2b_5T_5+4b_6T_6+4b_7T_7+4b_8T} + \left(\frac{2\pi\cos\theta}{rG}\right)^2, \tag{17b}$$

parameters c_i and d_i can be determined by minimizing the error function:

$$E = \iint (E_1^2 + E_2^2)\,d\tilde{k}\,d\theta, \tag{18}$$

where the ranges of θ and $\tilde{k}$ are the same as those in equation 11. Because c_i and d_i satisfy equation 7, only eight independent coefficients are solved from the optimization.

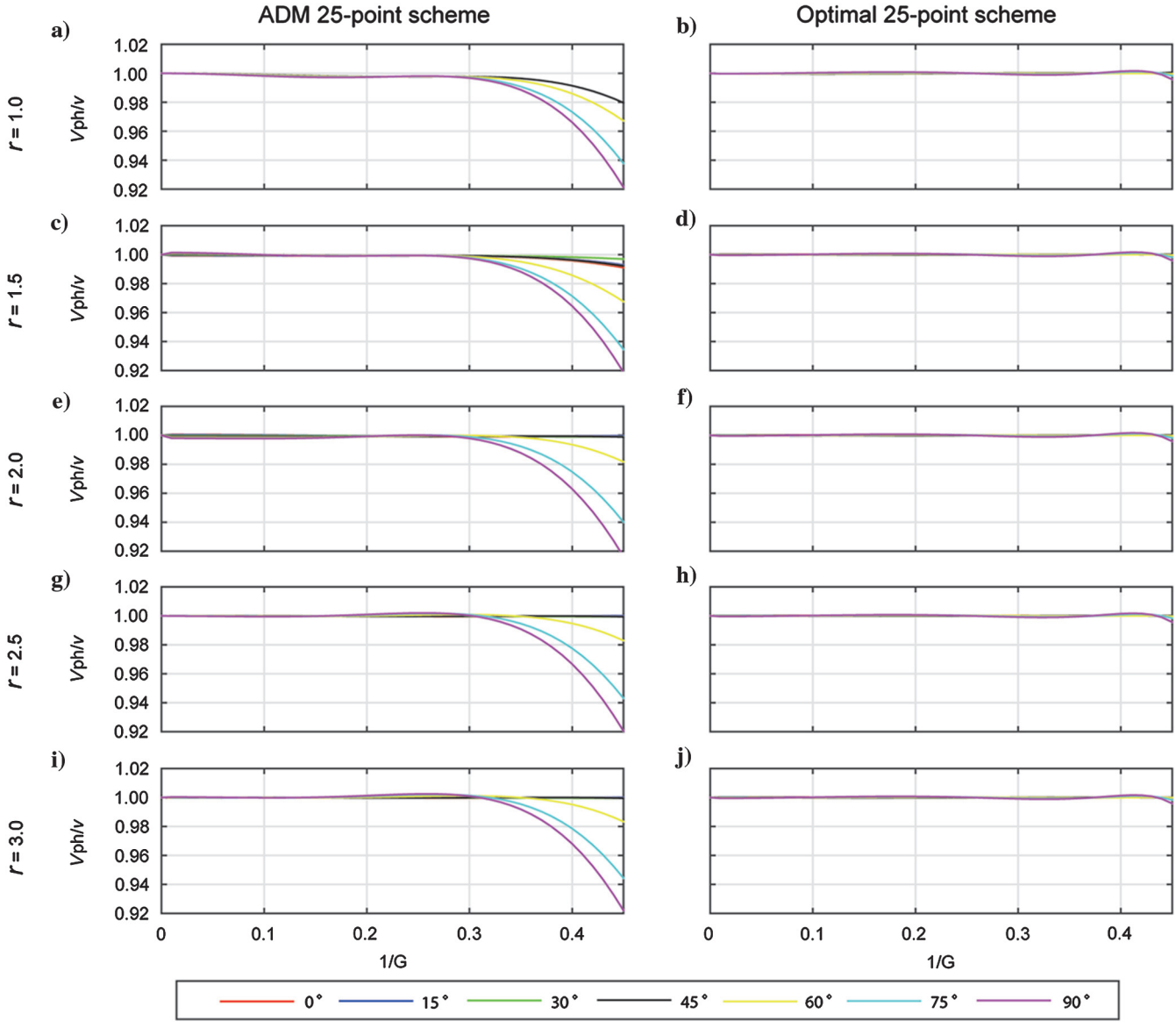

Figure 2. Normalized phase velocity curves for the ADM 25-point scheme (left column) and the optimal 25-point scheme proposed in this paper (right column). Rows from top to bottom are for $r = 1.0$, 1.5, 2.0, 2.5, and 3.0. The vertical coordinate is the normalized phase velocity, and the horizontal coordinate is $1/G$.

In brief, we first determine a_i and b_i $(i = 1, 2, \ldots, 8)$ by optimizing equation 11 and then determine c_i and d_i $(i = 1, 2, \ldots, 8)$ by optimizing equation 18. Only 24 independent coefficients are needed for the 25-point scheme. Objective functions 11 and 18 can be numerically calculated by summing up discretized integrands, where the range of θ is in $[0, \pi/2]$ at an interval of $\pi/200$, and the range of $\tilde{k}$ is in $[0, 0.45]$ at an interval of 0.0045. A constrained nonlinear optimization program, *fmincon*, in MATLAB is used in the optimization. The 24 optimized coefficients for different r are listed in Table 1.

Normalized phase velocity curves calculated from the ADM 25-point scheme (left column) are illustrated in Figure 2, and our optimized 25-point scheme (right column) based on coefficients is provided in Table 1. To keep the phase velocity error below 1%, the ADM 25-point scheme requires $G = 2.78$ (Zhang et al., 2015), whereas our optimized 25-point scheme requires $G = 2.13$. In other words, our scheme can reduce the computation cost by achieving the same accuracy with a coarse grid.

By selecting part of the grid points in the 25-point scheme, our optimal method can be used to investigate other FD schemes in Figure 1. In optimizing equations 11 and 18, the range of θ is always in $[0, \pi/2]$ and the range of $\tilde{k}$ depends on the number of grid points involved in the scheme. The more grid points that are involved, the larger the range of $\tilde{k}$ that should be used. Given an FD scheme, there is a trade-off between the wavenumber coverage and the phase velocity error. In this study, we used a trial-and-error method to

Table 2. Optimized coefficients for nine-point scheme, with different r values and $\Delta x \geq \Delta z$.

r	1.0	1.5	2.0	2.5	3.0
c_1	7.956000210E-01	7.922758570E-01	7.732513255E-01	7.451095721E-01	7.092571791E-01
c_2	−2.019816322E-01	−2.046614061E-01	−2.226356686E-01	−2.493232690E-01	−2.833551389E-01
c_3	1.013181335E-01	1.031377150E-01	1.126963178E-01	1.267816333E-01	1.447132971E-01
d_1	−2.019813204E-01	−1.920879426E-01	−1.904277620E-01	−1.899621523E-01	−1.897946553E-01
d_2	7.956003283E-01	8.075566877E-01	8.094786903E-01	8.099924931E-01	8.101685540E-01
d_3	1.013179603E-01	9.600883497E-02	9.517270403E-02	9.495073402E-02	9.487524596E-02
b_1	8.843341761E-02	9.403090272E-02	1.048256923E-01	1.194677370E-01	1.377227093E-01
b_2	8.843342121E-02	8.861014042E-02	9.743381289E-02	1.109688678E-01	1.283973422E-01
b_3	1.824034734E-03	−9.140586234E-04	−6.301797082E-03	−1.362019264E-02	−2.274672347E-02

Table 3. Optimized coefficients for 17-point scheme, with different r values and $\Delta x \geq \Delta z$.

r	1.0	1.5	2.0	2.5	3.0
c_1	5.176595449E-01	1.167271713E+00	7.854896834E-01	7.020072093E-01	6.969326319E-01
c_2	−2.631968183E-01	6.678359585E-01	3.739428150E-01	3.093095544E-01	3.077051987E-01
c_3	1.264963362E-01	−4.412257947E-01	−2.564888797E-01	−2.141660738E-01	-2.106783262E-01
c_4	5.542912726E-02	1.049840391E-01	1.426594047E-01	1.513582797E-01	1.535569321E-01
c_5	5.977493060E-03	4.222724353E-03	4.787745925E-03	4.784716103E-03	4.544972256E-03
c_8	−2.865044566E-04	3.876350114E-02	2.009591717E-02	1.527473162E-02	1.383508861E-02
d_1	−2.631958220E-01	−4.015004873E-01	−4.295541494E-01	−4.324364810E-01	−4.326982673E-01
d_2	5.176616509E-01	1.310066305E+00	1.061465437E+00	1.017895109E+00	1.031991880E+00
d_3	1.264956784E-01	2.005961891E-01	2.147969266E-01	2.162235877E-01	2.163492608E-01
d_4	5.977138978E-03	5.628545863E-03	−3.596268796E-03	−5.259826225E-03	−5.734422423E-03
d_5	5.542849487E-02	−1.830963639E-01	−1.286489886E-01	−1.186657138E-01	−1.222989046E-01
d_8	−2.861760616E-04	−3.616405714E-03	1.661635962E-03	2.596780928E-03	2.856818626E-03
b_1	1.115277121E-01	1.247463677E-01	1.595651183E-01	1.677510287E-01	1.700044697E-01
b_2	1.115275514E-01	-8.167334436E-02	-2.955752113E-02	-2.008356984E-02	−2.342622062E-02
b_3	2.012218218E-02	4.561371160E-02	2.894535914E-02	2.477279270E-02	2.352184165E-02
b_4	−4.852656851E-03	4.364743575E-03	8.452751975E-03	9.406179625E-03	9.843030443E-03
b_5	−4.852691375E-03	−2.784387153E-02	−1.857412132E-02	−1.628169867E-02	−1.558977805E-02
b_8	1.191254228E-04	3.704708819E-03	1.913889282E-03	1.431577743E-03	1.182758177E-03

choose a reasonable wavenumber coverage for different schemes. For the nine-point scheme (Figure 1b), by setting $c_i = d_i = 0$ $(i = 4, 5, 6, 7, 8)$ and the range of $\tilde{k}$ within $[0, 0.25]$, the obtained coefficients are listed in Table 2. Similarly, for the 17-point scheme (Figure 1c), setting $c_i = d_i = 0$ $(i = 6, 7)$ and $\tilde{k}$ within $[0, 0.4]$, the obtained coefficients are listed in Table 3. For the 15-point scheme (Figure 1d), setting $c_i = d_i = 0$ $(i = 5, 7, 8)$ and $\tilde{k}$ within $[0, 0.3]$, the coefficients are listed in Table 4. Compared with the corresponding ADM schemes, our results generally have higher accuracy, but the increments are trivial for 9-, 17-, and 15-point schemes.

For the case of $\Delta x < \Delta z$, due to the symmetric property of 25-, 9-, and 17-point schemes, we can obtain their parameters by exchanging parameters a_1, a_4, and a_6 with a_2, a_5, and a_7 in the $\Delta x \geq \Delta z$ result (Tang et al., 2015; Zhang et al., 2015). For the 15-point scheme, due to lack of the symmetry, their parameters need be recalculated. By setting $r = \Delta z/\Delta x$, $G = 2\pi/k\Delta z$, $a_i = r^2 c_i + d_i$ $(i = 0, 1, 2, \ldots, 8)$ and properly adjusting the corresponding optimization functions 11 and 18, the optimized coefficients for the 15-point scheme are listed in Table 5.

Table 4. Optimized coefficients for 15-point scheme, with different r values and $\Delta x \geq \Delta z$.

r	1.0	1.5	2.0	2.5	3.0
c_1	3.044652831E-01	3.294998210E-01	3.305953920E-01	3.309430830E-01	3.367777622E-01
c_2	−5.815191216E-02	−8.507101693E-02	−8.795537825E-02	−8.900878732E-02	−7.770338197E-02
c_3	3.296912669E-03	2.603107959E-02	2.927534196E-02	3.045045331E-02	2.264743850E-02
c_4	1.206034839E-01	1.213532509E-01	1.231216740E-01	1.237210754E-01	1.216479174E-01
c_6	2.582367375E-02	1.662016530E-02	1.479299529E-02	1.415915042E-02	1.641758773E-02
d_1	−3.829133302E-01	−3.971014384E-01	−3.995340373E-01	−4.000546654E-01	−4.024993530E-01
d_2	5.753976776E-01	5.811810402E-01	5.816458138E-01	5.819493910E-01	5.789703972E-01
d_3	1.904958260E-01	1.984753211E-01	1.997546742E-01	2.000262200E-01	2.012471618E-01
d_4	−3.925186444E-02	−2.106323175E-02	−1.859410404E-02	−1.788755680E-02	−1.845381848E-02
d_6	2.005198977E-02	1.056812040E-02	9.302870893E-03	8.944341341E-03	9.227398735E-03
b_1	1.423677300E-01	1.564692960E-01	1.610368776E-01	1.627902825E-01	1.599028305E-01
b_2	3.465580464E-02	4.544914079E-02	4.702674100E-02	4.753237188E-02	4.366382624E-02
b_3	3.529350134E-02	2.275283039E-02	1.987756711E-02	1.879204398E-02	2.095839546E-02
b_4	1.931735449E-02	1.112412580E-02	9.260043369E-03	8.665876298E-03	9.895769304E-03
b_6	−4.298251122E-03	−1.038504781E-03	−1.994632759E-04	6.387479298E-05	−4.184510005E-04

Table 5. Optimized coefficients for 15-point scheme, with different r values and $\Delta x < \Delta z$.

r	1.5	2.0	2.5	3.0
c_1	9.130050529E+00	2.955819531E+00	1.481966129E+00	4.953150127E+00
c_2	−1.572474857E+00	−1.541488855E-01	4.185906535E-01	−1.799711976E-01
c_3	1.013749155E+00	6.121881532E-02	−3.239391372E-01	7.852660027E-02
c_4	−2.089606364E+00	−5.528718760E-01	−1.887765176E-01	−1.050723370E+00
c_6	−2.262318935E-01	1.665119397E-02	1.154041346E-01	1.171217076E-02
d_1	3.235346450E+00	4.569687440E-01	−6.216963272E-01	1.055827007E+00
d_2	4.686368997E+00	1.575442510E+00	5.019299553E-01	2.291885651E+00
d_3	−1.667542954E+00	−2.393593723E-01	3.155868524E-01	−5.381586701E-01
d_4	3.923048754E-01	1.135937379E-01	1.427744152E-01	2.299016049E-01
d_6	−1.801102195E-01	−5.323532721E-02	−7.301450078E-02	−1.117934485E-01
b_1	−1.488022963E+00	−7.970738033E-01	−1.324006596E+00	−2.742547125E+00
b_2	2.426676984E-01	−2.965389041E-01	−9.994211782E-01	−1.465815174E+00
b_3	−1.000257708E-02	2.860914886E-01	7.411842859E-01	1.090875170E+00
b_4	−1.097667175E-01	1.255171575E-01	3.761716952E-01	5.223392792E-01
b_6	−6.309720678E-02	−8.951804085E-02	−1.931589514E-01	−3.096493266E-01

Expand to the 3D case

Here, we briefly discuss how to expand the method to the 3D case. From the 3D scalar wave equation,

$$\frac{\partial^2 P}{\partial x^2}+\frac{\partial^2 P}{\partial y^2}+\frac{\partial^2 P}{\partial z^2}+\frac{\omega^2}{v^2}P=0, \tag{19}$$

a 27-point scheme (Operto et al., 2007; Chen, 2014; Gosselin-Cliche and Giroux, 2014) in Figure 3 can be obtained as

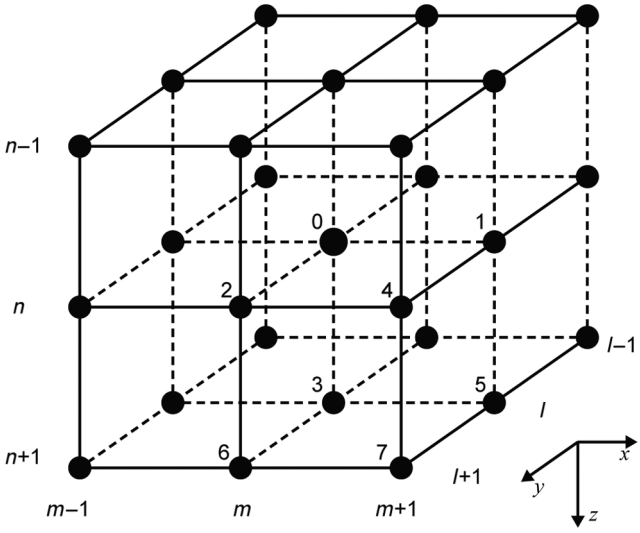

Figure 3. Cartoon showing the 27-point scheme for the 3D frequency-domain FD operator.

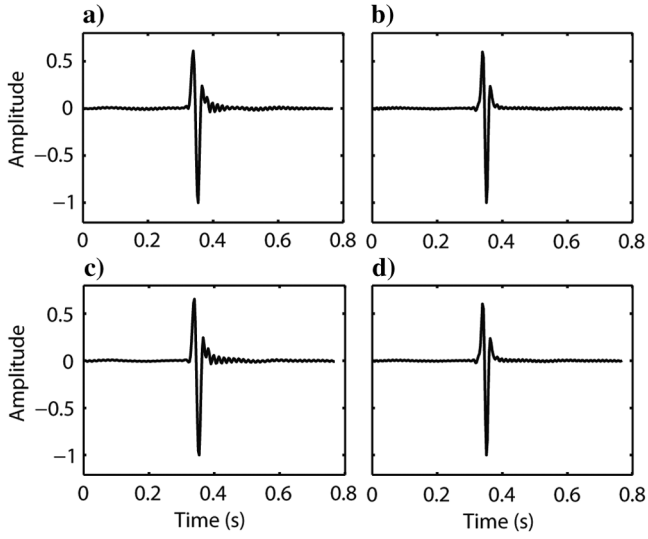

Figure 5. Synthetic seismograms calculated in the homogeneous model using the ADM 25-point scheme with (a) $r = 1.0$ and (c) $r = 2.0$, and the 25-point scheme proposed in this paper with (b) $r = 1.0$ and (d) $r = 2.0$.

Figure 4. Wavefield snapshots at $t = 540$ ms, calculated in a homogeneous model using the ADM 25-point scheme with (a) $r = 1.0$ and (c) $r = 2.0$, and the optimized 25-point scheme proposed in this paper with (b) $r = 1.0$ and (d) $r = 2.0$.

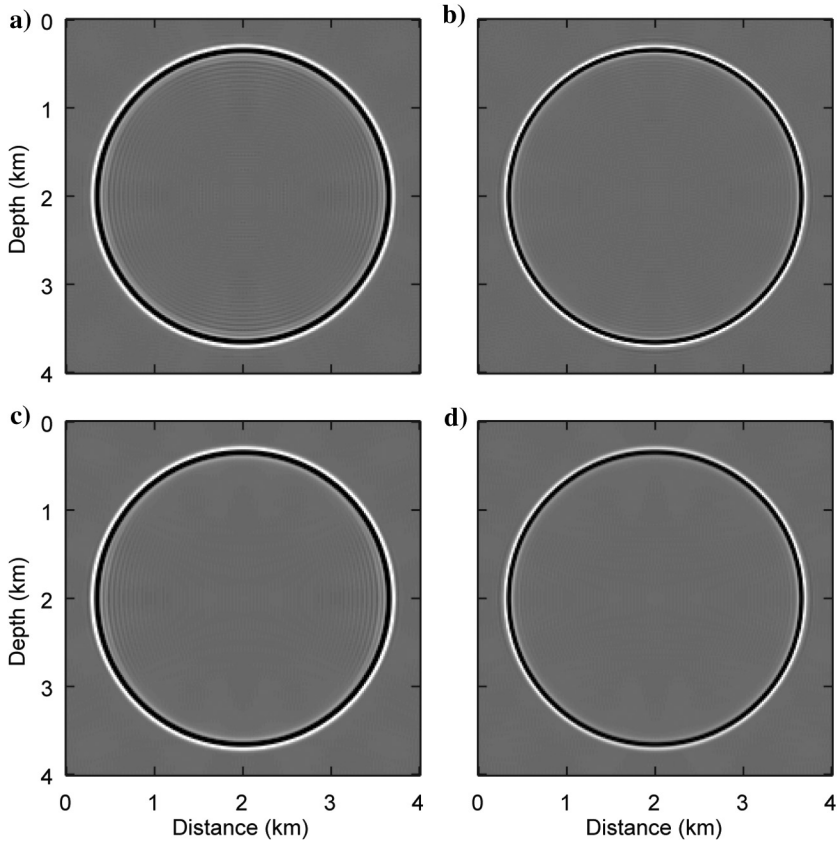

$$
\begin{aligned}
&\frac{1}{\Delta x^2}[c_0P_{m,l,n}+c_1(P_{m-1,l,n}+P_{m+1,l,n})+c_2(P_{m,l-1,n}+P_{m,l+1,n})+c_3(P_{m,l,n-1}+P_{m,l,n+1})\\
&+c_4(P_{m-1,l-1,n}+P_{m+1,l+1,n}+P_{m-1,l+1,n}+P_{m+1,l-1,n})\\
&+c_5(P_{m-1,l,n-1}+P_{m+1,l,n+1}+P_{m-1,l,n+1}+P_{m+1,l,n-1})\\
&+c_6(P_{m,l-1,n-1}+P_{m,l+1,n+1}+P_{m,l-1,n+1}+P_{m,l+1,n-1})\\
&+c_7(P_{m-1,l-1,n-1}+P_{m+1,l-1,n-1}+P_{m-1,l+1,n-1}+P_{m+1,l+1,n-1}+P_{m-1,l-1,n+1}\\
&+P_{m+1,l-1,n+1}+P_{m-1,l+1,n+1}+P_{m+1,l+1,n+1})]\\
&+\frac{1}{\Delta y^2}[e_0P_{m,l,n}+e_1(P_{m-1,l,n}+P_{m+1,l,n})+e_2(P_{m,l-1,n}+P_{m,l+1,n})+e_3(P_{m,l,n-1}+P_{m,l,n+1})\\
&+e_4(P_{m-1,l-1,n}+P_{m+1,l+1,n}+P_{m-1,l+1,n}+P_{m+1,l-1,n})\\
&+e_5(P_{m-1,l,n-1}+P_{m+1,l,n+1}+P_{m-1,l,n+1}+P_{m+1,l,n-1})\\
&+e_6(P_{m,l-1,n-1}+P_{m,l+1,n+1}+P_{m,l-1,n+1}+P_{m,l+1,n-1})\\
&+e_7(P_{m-1,l-1,n-1}+P_{m+1,l-1,n-1}+P_{m-1,l+1,n-1}+P_{m+1,l+1,n-1}+P_{m-1,l-1,n+1}\\
&+P_{m+1,l-1,n+1}+P_{m-1,l+1,n+1}+P_{m+1,l+1,n+1})]\\
&+\frac{1}{\Delta z^2}[d_0P_{m,l,n}+d_1(P_{m-1,l,n}+P_{m+1,l,n})+d_2(P_{m,l-1,n}+P_{m,l+1,n})+e_3(P_{m,l,n-1}+P_{m,l,n+1})\\
&+d_4(P_{m-1,l-1,n}+P_{m+1,l+1,n}+P_{m-1,l+1,n}+P_{m+1,l-1,n})\\
&+d_5(P_{m-1,l,n-1}+P_{m+1,l,n+1}+P_{m-1,l,n+1}+P_{m+1,l,n-1})\\
&+d_6(P_{m,l-1,n-1}+P_{m,l+1,n+1}+P_{m,l-1,n+1}+P_{m,l+1,n-1})\\
&+d_7(P_{m-1,l-1,n-1}+P_{m+1,l-1,n-1}+P_{m-1,l+1,n-1}+P_{m+1,l+1,n-1}+P_{m-1,l-1,n+1}\\
&+P_{m+1,l-1,n+1}+P_{m-1,l+1,n+1}+P_{m+1,l+1,n+1})]\\
&+\frac{\omega^2}{v^2}[b_0P_{m,l,n}+b_1(P_{m-1,l,n}+P_{m+1,l,n})+b_2(P_{m,l-1,n}+P_{m,l+1,n})+b_3(P_{m,l,n-1}+P_{m,l,n+1})\\
&+b_4(P_{m-1,l-1,n}+P_{m+1,l+1,n}+P_{m-1,l+1,n}+P_{m+1,l-1,n})\\
&+b_5(P_{m-1,l,n-1}+P_{m+1,l,n+1}+P_{m-1,l,n+1}+P_{m+1,l,n-1})\\
&+b_6(P_{m,l-1,n-1}+P_{m,l+1,n+1}+P_{m,l-1,n+1}+P_{m,l+1,n-1})\\
&+b_7(P_{m-1,l-1,n-1}+P_{m+1,l-1,n-1}+P_{m-1,l+1,n-1}+P_{m+1,l+1,n-1}\\
&+P_{m-1,l-1,n+1}+P_{m+1,l-1,n+1}+P_{m-1,l+1,n+1}+P_{m+1,l+1,n+1})]=0, \qquad (20)
\end{aligned}
$$

where $P_{m,l,n} = P(m\Delta x, l\Delta y, n\Delta z)$ and Δx, Δy, and Δz are the spatial sampling intervals in the x-, y-, and z-directions, respectively. The functions c_i, e_i, d_i, and b_i are the weighting coefficients to approximate $\partial^2P/\partial x^2$, $\partial^2P/\partial y^2$, $\partial^2P/\partial z^2$ and mass acceleration term, and they satisfy the following relationships:

$$c_0 + 2c_1 + 2c_2 + 2c_3 + 4c_4 + 4c_5 + 4c_6 + 8c_7 = 0, \quad (21)$$

$$e_0 + 2e_1 + 2e_2 + 2e_3 + 4e_4 + 4e_5 + 4e_6 + 8e_7 = 0, \quad (22)$$

$$d_0+2d_1+2d_2+2d_3+4d_4+4d_5+4d_6+8d_7=0, \quad (23)$$

and

$$b_0+2b_1+2b_2+2b_3+4b_4+4b_5+4b_6+8b_7=1. \quad (24)$$

Given $\Delta x=\max(\Delta x,\Delta y,\Delta z)$, we define $r_1=\Delta x/\Delta y$, $r_2 = \Delta x/\Delta z$ and set

$$a_i = c_i + r_1^2e_i + r_2^2d_i (i = 0, 1, 2, \ldots, 7), \quad (25)$$

where a_i satisfy $a_0 + 2a_1 + 2a_2 + 2a_3 + 4a_4 + 4a_5 + 4a_6 + 8a_7 = 0$. Similar to dealing with equation 8, the 27-point 3D scheme can be expressed in a concise form, with their coefficients c_i, e_i, d_i, and b_i optimized in a way similar to that used in the 2D case.

NUMERICAL EXAMPLES

We present two 2D numerical examples to validate the accuracy of our 25-point scheme. In the first example, we use the ADM 25-point scheme and our scheme to calculate scalar wave propagation in a 4×4 km homogeneous velocity model of 3.5 km/s. The source is located at the center of the model, and the source time

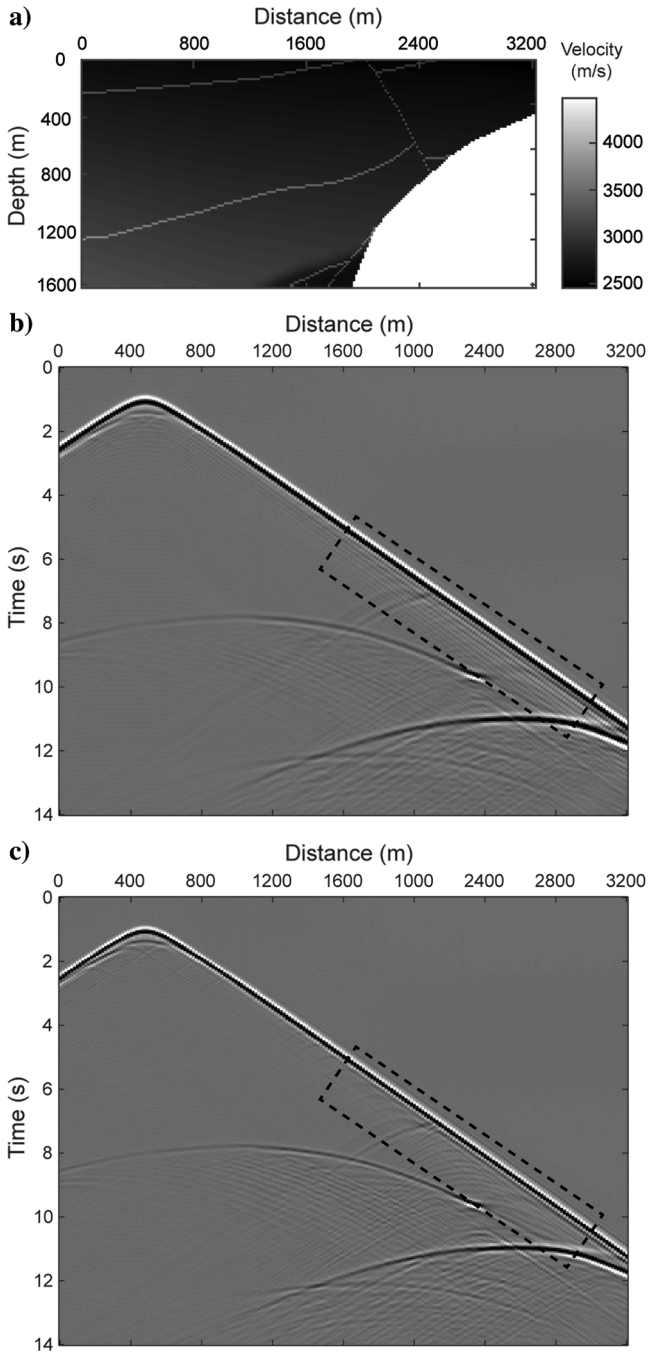

Figure 6. Heterogeneous velocity model and synthetic shot gathers, with (a) part of the SEG/EAGE salt model, (b and c) synthetic seismograms calculated using the ADM 25-point scheme and the optimized 25-point scheme proposed in this paper. The dashed rectangles indicate regions with apparent differences.

function is a 30 Hz Ricker wavelet. We test two different grids. The first uses equal grid space with $dx = dz = 20\ m$ ($r = 1.0$), and the resulting grid is 201×201. The second uses a rectangular grid with $dx = 20\ m$ and $dz = 10\ m$ ($r = 2.0$), and the resulted grid is 201×401. We use the open-source software MUMPS (multifrontal massively parallel solver, Amestoy et al., 2001, 2006) to solve the sparse linear system. Figure 4 compares the snapshots at $t =$ 540 ms calculated using different methods and different aspect ratios r, in which Figure 4a and 4c is calculated using an ADM 25-point scheme with $r = 1.0$ and $r = 2.0$, and Figure 4b and 4d is calculated using the scheme proposed in this paper with $r = 1.0$ and $r = 2.0$. Apparently, the results from our scheme show weaker numerical dispersions than those calculated using the ADM 25-point scheme. To compare synthetic waveforms, a receiver located 1000 m to the right of the source is used. Figure 5 shows four seismograms, in which Figure 5a–5d is arranged in the same order as in Figure 4. We see that our 25-point scheme generates weaker numerical dispersions than the ADM scheme for $r = 1.0$ and $r = 2.0$.

The second example is for a heterogeneous model, which is part of the SEG/EAGE salt model as shown in Figure 6a. The sampling intervals are $dx = dz = 16$ m, and the number of grids is 201×101. The source, a 30 Hz Ricker wavelet, is placed at ($x = 480$ m, $z = 48$ m), and the receivers are set at the depth of 160 m and extended horizontally to the entire model. Synthetic seismograms computed with the ADM 25-point scheme and our 25-point scheme are shown in Figure 6b and 6c, respectively. Apparently, the result from our method shows much weaker dispersions compared with that from the ADM method, particularly in regions highlighted by the dashed rectangles. For 9-, 17-, and 15-point schemes, numerical experiments (not shown here) demonstrate that our optimal method gives similar accuracy to that from corresponding ADM schemes.

CONCLUSION

We propose a new optimal method for frequency-domain FD modeling. The main advantage of this new method is its generality and flexibility, with which we can directly construct the dispersion equations and determine the coefficients once the FD stencil is given. Under this framework, optimized coefficients of 9-, 17-, and 15-point schemes can be calculated as special cases of the 25-point scheme. From dispersion analysis, our 25-point scheme has much higher accuracy than the ADM 25-point scheme. The number of grid points per the smallest wavelength is reduced from 2.78 to 2.13 given the maximum phase velocity errors less than 1%. The possibility of expanding this method to the 3D case is briefly discussed. The optimized coefficients for 25-, 9-, 17-, and 15-point schemes are presented. To validate the optimal method, two numerical examples are presented: The first is a homogeneous model, and the second is a model with a salt body. The results show that the synthetic seismograms and the snapshots generated using our optimal 25-point scheme have smaller dispersions than that generated using the ADM 25-point scheme.

ACKNOWLEDGMENTS

Associate editor S. O. Hestholm and the seven reviewers are appreciated for their critical comments that greatly improved this manuscript. The authors wish to thank J.-W. Cheng for fruitful discussions in the numerical modeling. This research was supported by the National Natural Science Foundation of China (grant nos. 41604037, 41504102, 41674107, and 41674060) and the Open Research Fund Program of the Key Laboratory of Geospace Environment and Geodesy (Wuhan University), Ministry of Education (no. 15-01-02).

APPENDIX A

RELATIONS BETWEEN OUR SCHEME AND OTHER COMMONLY USED SCHEMES

Our scheme described in equation 5 is a general formula, which can include many commonly used schemes for frequency-domain 2D scalar wave modeling as special cases under a unified framework.

If we assign

$$\begin{aligned} &c_1 = 1, c_i = 0 \quad (i = 2,3,4,5,6,7,8),\\ &d_2 = 1, d_i = 0 \quad (i = 1,3,4,5,6,7,8),\\ &b_i = 0 \quad (i = 1,2,3,4,5,6,7,8), \end{aligned} \tag{A-1}$$

equation 5 becomes the classic five-point scheme.

If we assign

$$\begin{aligned} &c_1 = \frac{4}{3}, \quad c_4 = -\frac{1}{12}, \quad c_i = 0 \quad (i = 2,3,5,6,7,8),\\ &d_2 = \frac{4}{3}, \quad d_5 = -\frac{1}{12}, \quad d_i = 0 \quad (i = 1,3,4,6,7,8),\\ &b_i = 0 \quad (i = 1,2,3,4,5,6,7,8), \end{aligned} \tag{A-2}$$

equation 5 becomes the classic nine-point scheme.

For $\Delta x = \Delta z$ ($r = 1.0$), if we combine the similar terms in equation 5 and let

$$\begin{aligned} &c_1 + d_1 = a^{\mathrm{Jo}},\ c_2 + d_2 = a^{\mathrm{Jo}},\ c_3 + d_3 = \frac{1 - a^{\mathrm{Jo}}}{2},\\ &c_i = d_i = 0\ (i = 4,5,6,7,8),\\ &b_1 = b_2 = d^{\mathrm{Jo}},\ b_3 = \frac{1 - c^{\mathrm{Jo}} - 4d^{\mathrm{Jo}}}{4},\ b_i = 0\ (i = 4,5,6,7,8), \end{aligned} \tag{A-3}$$

where $a^{\mathrm{Jo}} = 0.5461$, $c^{\mathrm{Jo}} = 0.6248$, and $d^{\mathrm{Jo}} = 0.09381$ are the optimized coefficients by Jo et al. (1996), equation 5 becomes the rotated nine-point scheme.

For $\Delta x = \Delta z (r = 1.0)$, if we assign

$$\begin{aligned} &c_1 + d_1 = c_2 + d_2 = a_1^{\mathrm{Shin}}, \quad c_3 + d_3 = a_2^{\mathrm{Shin}},\\ &c_4 + d_4 = c_5 + d_5 = a_3^{\mathrm{Shin}},\\ &c_6 + d_6 = a_5^{\mathrm{Shin}}, \quad c_7 + d_7 = a_6^{\mathrm{Shin}}, \quad c_8 + d_8 = a_4^{\mathrm{Shin}},\\ &b_0 = b_1^{\mathrm{Shin}}, \quad b_1 = b_2 = b_2^{\mathrm{Shin}}, \quad b_3 = b_4^{\mathrm{Shin}},\\ &b_4 = b_5 = b_3^{\mathrm{Shin}}, \quad b_6 = b_6^{\mathrm{Shin}}, \quad b_7 = b_7^{\mathrm{Shin}}, \quad b_8 = b_5^{\mathrm{Shin}}, \end{aligned} \tag{A-4}$$

where $a_1^{\mathrm{Shin}} = 0.0949098$, $a_2^{\mathrm{Shin}} = 0.280677$, $a_3^{\mathrm{Shin}} = 0.247253$, $a_4^{\mathrm{Shin}} = 0.0297441$, $a_5^{\mathrm{Shin}} = 0.173708$, $a_6^{\mathrm{Shin}} = 0.173708$, $b_1^{\mathrm{Shin}} =$

0.363276, $b_2^{\text{Shin}} = 0.108598$, $b_3^{\text{Shin}} = 0.00414870$, $b_4^{\text{Shin}} = 0.0424801$, $b_5^{\text{Shin}} = 0.000206312$, $b_6^{\text{Shin}} = 0.00187765$, and $b_7^{\text{Shin}} = 0.00188342$ are the optimized coefficients by Shin and Sohn (1998), equation 5 becomes the rotated 25-point scheme.

For $\Delta x = \Delta z (r = 1.0)$, if we assign

$$
\begin{aligned}
&c_1 + d_1 = c_2 + d_2 = \frac{4}{3}a^{\text{Cao}}, \quad c_3 + d_3 = \frac{4}{3}(1 - a^{\text{Cao}}),\\
&c_4 + d_4 = c_5 + d_5 = -\frac{1}{12}a^{\text{Cao}},\\
&c_6 = d_6 = c_7 = d_7 = 0, \quad c_8 + d_8 = -\frac{1}{12}(1 - a^{\text{Cao}}),\\
&b_0 = b^{\text{Cao}}, \quad b_1 = b_2 = c^{\text{Cao}}, \quad b_3 = d^{\text{Cao}},\\
&b_4 = b_5 = e^{\text{Cao}}, \quad b_6 = b_7 = 0, \quad b_8 = f^{\text{Cao}}, \qquad \text{(A-5)}
\end{aligned}
$$

where $a^{\text{Cao}} = 1.0673$, $b^{\text{Cao}} = 0.8875$, $c^{\text{Cao}} = 0.0251$, $d^{\text{Cao}} = 0.0237$, and $e^{\text{Cao}} = -0.0204$ are the optimized coefficients by Cao and Chen (2012), and f^{Cao} satisfies $b^{\text{Cao}} + 4c^{\text{Cao}} + 4d^{\text{Cao}} + 4e^{\text{Cao}} + 4f^{\text{Cao}} = 1$, equation 5 becomes the rotated 17-point scheme.

If we assign

$$
\begin{aligned}
&c_1 = \alpha^{\text{Chen}}, \quad c_2 = \alpha^{\text{Chen}} - 1, \quad c_2 = \frac{1 - \alpha^{\text{Chen}}}{2},\\
&c_i = 0 \quad (i = 4, 5, 6, 7, 8),\\
&d_1 = \beta^{\text{Chen}} - 1, \quad d_2 = \beta^{\text{Chen}}, \quad d_2 = \frac{1 - \beta^{\text{Chen}}}{2},\\
&d_i = 0 \quad (i = 4, 5, 6, 7, 8),\\
&b_1 = d^{\text{Chen}}, \quad b_2 = d^{\text{Chen}}, \quad b_3 = \frac{1 - c^{\text{Chen}} - 4d^{\text{Chen}}}{4},\\
&b_i = 0 \quad (i = 4, 5, 6, 7, 8), \qquad \text{(A-6)}
\end{aligned}
$$

where α^{Chen}, β^{Chen}, c^{Chen}, and d^{Chen} are the optimized coefficients by Chen (2012) and their values are dependent on r, equation 5 becomes the ADM nine-point scheme.

In equation 5, we assign

$$
\begin{aligned}
&c_1 = \frac{4}{3}\alpha_1^{\text{Zhang}}, \; c_2 = -\frac{5}{2}\alpha_2^{\text{Zhang}}, \; c_3 = \frac{4}{3}\alpha_2^{\text{Zhang}}, \; c_4 = -\frac{1}{12}\alpha_1^{\text{Zhang}},\\
&c_5 = -\frac{5}{2}\alpha_3^{\text{Zhang}}, \; c_6 = -\frac{1}{12}\alpha_2^{\text{Zhang}}, \; c_7 = \frac{4}{3}\alpha_3^{\text{Zhang}}, \; c_8 = -\frac{1}{12}\alpha_3^{\text{Zhang}},\\
&d_1 = -\frac{5}{2}\beta_2^{\text{Zhang}}, \; d_2 = \frac{4}{3}\beta_1^{\text{Zhang}}, \; d_3 = \frac{4}{3}\beta_2^{\text{Zhang}}, \; d_4 = -\frac{5}{2}\beta_3^{\text{Zhang}},\\
&d_5 = -\frac{1}{12}\beta_1^{\text{Zhang}}, \; d_6 = \frac{4}{3}\beta_3^{\text{Zhang}}, \; d_7 = -\frac{1}{12}\beta_2^{\text{Zhang}}, \; d_8 = -\frac{1}{12}\beta_3^{\text{Zhang}},\\
&b_0 = b_1^{\text{Zhang}}, \; b_1 = b_2^{\text{Zhang}}, \; b_2 = b_3^{\text{Zhang}}, \; b_3 = b_6^{\text{Zhang}}, \; b_4 = b_4^{\text{Zhang}},\\
&b_5 = b_5^{\text{Zhang}}, \; b_6 = b_8^{\text{Zhang}}, \; b_7 = b_9^{\text{Zhang}}, \; b_8 = b_7^{\text{Zhang}}, \qquad \text{(A-7)}
\end{aligned}
$$

where α_1^{Zhang}, α_2^{Zhang}, α_3^{Zhang}, β_1^{Zhang}, β_2^{Zhang}, β_3^{Zhang}, and b_i^{Zhang} $(i = 1, 2, \ldots, 9)$ are the optimized coefficients by Zhang et al. (2014), and their values are dependent on aspect ratio r, and they satisfy

$$
\begin{aligned}
&\alpha_1^{\text{Zhang}} + 2\alpha_2^{\text{Zhang}} + 2\alpha_3^{\text{Zhang}} = 1,\\
&\beta_1^{\text{Zhang}} + 2\beta_2^{\text{Zhang}} + 2\beta_3^{\text{Zhang}} = 1,\\
&b_1^{\text{Zhang}} + 2\sum_{i=2}^{5} b_i^{\text{Zhang}} + 4\sum_{i=6}^{9} b_i^{\text{Zhang}} = 1. \qquad \text{(A-8)}
\end{aligned}
$$

Under this circumstance, equation 5 becomes the ADM 25-point scheme.

We assign

$$
\begin{aligned}
&c_1 = \frac{4}{3}\alpha_2^{\text{Tang}}, \; c_2 = -\frac{5}{2}\alpha_4^{\text{Tang}}, \; c_3 = \frac{2}{3}(1 - \alpha_2^{\text{Tang}}), \; c_4 = -\frac{1}{12}\alpha_1^{\text{Tang}},\\
&c_5 = -\frac{5}{4}(1 - \alpha_3^{\text{Tang}} - 2\alpha_4^{\text{Tang}}), \; c_6 = c_7 = 0, \; c_8 = -\frac{1}{24}(1 - \alpha_1^{\text{Tang}}),\\
&d_1 = -\frac{5}{2}\beta_4^{\text{Tang}}, \; d_2 = \frac{4}{3}\beta_2^{\text{Tang}}, \; d_3 = \frac{2}{3}(1 - \beta_2^{\text{Tang}}),\\
&d_4 = -\frac{5}{4}(1 - \beta_3^{\text{Tang}} - 2\beta_4^{\text{Tang}}),\\
&d_5 = -\frac{1}{12}\beta_1^{\text{Tang}}, \; d_6 = d_7 = 0, \; d_8 = -\frac{1}{24}(1 - \beta_1^{\text{Tang}}),\\
&b_0 = b^{\text{Tang}}, \; b_1 = b_2 = c^{\text{Tang}}, \; b_3 = d^{\text{Tang}},\\
&b_4 = b_5 = e^{\text{Tang}}, \; b_6 = b_7 = 0, \; b_8 = f^{\text{Tang}}, \qquad \text{(A-9)}
\end{aligned}
$$

where $\alpha_1^{\text{Tang}}, \alpha_2^{\text{Tang}}, \alpha_3^{\text{Tang}}, \alpha_4^{\text{Tang}}, \beta_1^{\text{Tang}}, \beta_2^{\text{Tang}}, \beta_3^{\text{Tang}}, \beta_4^{\text{Tang}}, b^{\text{Tang}}, c^{\text{Tang}}, d^{\text{Tang}}, e^{\text{Tang}}$, and f^{Tang} are the optimized coefficients by Tang et al. (2015), with their values that are dependent on the aspect ratio r, and satisfy $b^{\text{Tang}} + 4c^{\text{Tang}} + 4d^{\text{Tang}} + 4e^{\text{Tang}} + 4f^{\text{Tang}} = 1$. Under this circumstance, equation 5 becomes the ADM 17-point scheme.

If we assign

$$
\begin{aligned}
&c_1 = c^{\text{Liu}}b_1^{\text{Liu}}, \; c_2 = -2c^{\text{Liu}}b_2^{\text{Liu}} - 2d^{\text{Liu}}b_2^{\text{Liu}},\\
&c_3 = c^{\text{Liu}}b_2^{\text{Liu}}, \; c_4 = d^{\text{Liu}}b_1^{\text{Liu}},\\
&c_5 = 0, \; c_6 = d^{\text{Liu}}b_2^{\text{Liu}}, \; c_7 = c_8 = 0,\\
&d_1 = -2e_2^{\text{Liu}}, \; d_2 = e_1^{\text{Liu}}, \; d_3 = e_2^{\text{Liu}}, \; d_4 = -2e_3^{\text{Liu}},\\
&d_5 = 0, \; d_6 = e_3^{\text{Liu}}, \; d_7 = d_8 = 0,\\
&b_0 = a_1^{\text{Liu}}, \; b_1 = b_2 = a_2^{\text{Liu}}, \; b_3 = a_3^{\text{Lin}}, \; b_4 = a_4^{\text{Liu}},\\
&b_5 = 0, \; b_6 = a_5^{\text{Liu}}, \; b_7 = b_8 = 0, \qquad \text{(A-10)}
\end{aligned}
$$

where b_1^{Liu}, b_2^{Liu}, e_1^{Liu}, e_2^{Liu}, e_3^{Liu}, c^{Liu}, d^{Liu}, a_1^{Liu}, a_2^{Liu}, a_3^{Liu}, a_4^{Liu}, and a_5^{Liu} are the optimized coefficients by Liu et al. (2013), equation 5 becomes the 15-point scheme. Liu et al. (2013) only consider the case $\Delta x = \Delta z$, but their method can be extended to deal with arbitrary aspect ratio r.

Therefore, these commonly used schemes, e.g., classic 5-point, classic 9-point, rotated 9-point, rotated 25-point, rotated 17-point, ADM 9-point, ADM 25-point, ADM 17-point, and 15-point schemes, can all be derived from equation 5 as special cases.

APPENDIX B

PML BOUNDARY CONDITION

For simplicity, we first give the PML on the boundary with its outer normal toward the positive x-direction and assume that the

PML starts from $x = 0$. Based on the concept of complex coordinate stretching, the equations within the PML layer have exactly the same form as in the physical domain $x < 0$, except the coordinate x is replaced with a complex stretched coordinate $\tilde{x}$:

$$\tilde{x} = \int_0^x s_x(\eta) d\eta. \tag{B-1}$$

In standard PML condition,

$$s_x(x) = 1 + \frac{d_x(x)}{i\omega}, \tag{B-2}$$

where $d_x(x)$ is the attenuation factor that causes the wave amplitude to reduce exponentially inside the PML layer. From equations B-1 and B-2, we have

$$\frac{\partial}{\partial \tilde{x}} = \frac{1}{s_x}\frac{\partial}{\partial x} \tag{B-3}$$

and

$$\frac{\partial^2}{\partial \tilde{x}^2} = \frac{1}{s_x^2}\frac{\partial^2}{\partial x^2} - \frac{1}{s_x^3}\frac{d'(x)}{i\omega}\frac{\partial}{\partial x}. \tag{B-4}$$

In equation B-4, the second term on the right side can be neglected while still properly absorbing the unwanted reflections. Therefore, we have

$$\frac{\partial^2}{\partial \tilde{x}^2} \approx \frac{1}{s_x^2}\frac{\partial^2}{\partial x^2}. \tag{B-5}$$

Equations B-4 and B-5 also work along the negative x-direction. Similarly, in the z-direction, we have

$$\frac{\partial^2}{\partial \tilde{z}^2} \approx \frac{1}{s_z^2}\frac{\partial^2}{\partial z^2}. \tag{B-6}$$

Combining equations B-5 and B-6, we have the wave equation within the PML layer as

$$\frac{1}{s_x^2}\frac{\partial^2 P}{\partial x^2} + \frac{1}{s_z^2}\frac{\partial^2 P}{\partial z^2} + \frac{\omega^2}{v^2}P = 0. \tag{B-7}$$

REFERENCES

Amestoy, P. R., I. S. Duff, J. Y. L'Excellent, and J. Koster, 2001, A fully asynchronous multifrontal solver using distributed dynamic scheduling: SIAM Journal on Matrix Analysis and Applications, **23**, 15–41, doi: 10.1137/S0895479899358194.

Amestoy, P. R., A. Guermouche, J. Y. L'Excellent, and S. Pralet, 2006, Hybrid scheduling for the parallel solution of linear systems: Parallel computing, **32**, 136–156, doi: 10.1016/j.parco.2005.07.004.

Berenger, J.-P., 1994, A perfectly matched layer for the absorption of electromagnetic waves: Journal of Computational Physics, **114**, 185–200.

Brossier, R., S. Operto, and J. Virieux, 2009, Seismic imaging of complex onshore structures by 2D elastic frequency-domain full-waveform inversion: Geophysics, **74**, no. 6, WCC105–WCC118, doi: 10.1190/1.3215771.

Cao, S.-H., and J.-B. Chen, 2012, A 17-point scheme and its numerical implementation for high-accuracy modeling of frequency-domain acoustic equation (in Chinese): Chinese Journal of Geophysics, **55**, 3440–3449, doi: 10.6038/cjg20140724.

Chen, J.-B., 2012, An average-derivative optimal scheme for frequency-domain scalar wave equation: Geophysics, **77**, no. 6, T201–T210, doi: 10.1190/geo2011-0389.1.

Chen, J.-B., 2014, A 27-point scheme for a 3D frequency-domain scalar wave equation based on an average-derivative method: Geophysical Prospecting, **62**, 258–277, doi: 10.1111/1365-2478.12090.

Chen, J.-B., and J. Cao, 2016, Modeling of frequency-domain elastic-wave equation with an average-derivative optimal method: Geophysics, **81**, no. 6, T339–T356, doi: 10.1190/geo2016-0041.1.

Gosselin-Cliche, B., and B. Giroux, 2014, 3D frequency-domain finite-difference viscoelastic-wave modeling using weighted average 27-point operators with optimal coefficients: Geophysics, **79**, no. 3, T169–T188, doi: 10.1190/geo2013-0368.1.

Holberg, O., 1987, Computational aspects of the choice of operator and sampling interval for numerical differentiation in large-scale simulation of wave phenomena: Geophysical Prospecting, **35**, 629–655, doi: 10.1111/j.1365-2478.1987.tb00841.x.

Hustedt, B., S. Operto, and J. Virieux, 2004, Mixed-grid and staggered-grid finite-difference methods for frequency-domain acoustic wave modelling: Geophysical Journal International, **157**, 1269–1296, doi: 10.1111/j.1365-246X.2004.02289.x.

Jo, C.-H., C. Shin, and J. H. Suh, 1996, An optimal 9-point, finite-difference, frequency-space, 2-D scalar wave extrapolator: Geophysics, **61**, 529–537, doi: 10.1190/1.1443979.

Li, Y., L. Métivier, R. Brossier, B. Han, and J. Virieux, 2015, 2D and 3D frequency-domain elastic wave modeling in complex media with a parallel iterative solver: Geophysics, **80**, no. 3, T101–T118, doi: 10.1190/geo2014-0480.1.

Liu, L., H. Liu, and H. Liu, 2013, Optimal 15-point finite difference forward modeling in frequency-space domain (in Chinese): Chinese Journal of Geophysics, **56**, 644–652, doi: 10.6038/cjg20130228.

Liu, Y., and M. K. Sen, 2009, A new time-space domain high-order finite-difference method for the acoustic wave equation: Journal of Computational Physics, **228**, 8779–8806, doi: 10.1016/j.jcp.2009.08.027.

Operto, S., R. Brossier, L. Combe, L. Métivier, A. Ribodetti, and J. Virieux, 2014, Computationally efficient three-dimensional acoustic finite-difference frequency-domain seismic modeling in vertical transversely isotropic media with sparse direct solver: Geophysics, **79**, no. 5, T257–T275, doi: 10.1190/geo2013-0478.1.

Operto, S., J. Virieux, P. Amestoy, J.-Y. L'Excellent, L. Giraud, and H. B. H. Ali, 2007, 3D finite-difference frequency-domain modeling of visco-acoustic wave propagation using a massively parallel direct solver: A feasibility study: Geophysics, **72**, no. 5, SM195–SM211, doi: 10.1190/1.2759835.

Operto, S., J. Virieux, A. Ribodetti, and J. E. Anderson, 2009, Finite-difference frequency-domain modeling of viscoacoustic wave propagation in 2D tilted transversely isotropic (TTI) media: Geophysics, **74**, no. 5, T75–T95, doi: 10.1190/1.3157243.

Pratt, R. G., 1999, Seismic waveform inversion in the frequency domain: Part 1 — Theory and verification in a physical scale model: Geophysics, 901–888 ,**64**, doi: 10.1190/1.1444597.

Pratt, R. G., and M. Worthington, 1990, Inverse theory applied to multi-source cross-hole tomography: Part 1 — Acoustic wave-equation method: Geophysical Prospecting, **38**, 287–310, doi: 10.1111/j.1365-2478.1990.tb01846.x.

Shin, C., and H. Sohn, 1998, A frequency-space 2-D scalar wave extrapolator using extended 25-point finite-difference operator: Geophysics, **63**, 289–296, doi: 10.1190/1.1444323.

Štekl, I., and R. G. Pratt, 1998, Accurate viscoelastic modeling by frequency-domain finite differences using rotated operators: Geophysics, **63**, 1779–1794, doi: 10.1190/1.444472.

Tang, X., H. Liu, H. Zhang, L. Liu, and Z. Wang, 2015, An adaptable 17-point scheme for high-accuracy frequency-domain acoustic wave modeling in 2D constant density media: Geophysics, **80**, no. 6, T211–T221, doi: 10.1190/geo2014-0124.1.

Virieux, J., and S. Operto, 2009, An overview of full-waveform inversion in exploration geophysics: Geophysics, **74**, no. 6, WCC1–WCC26, doi: 10.1190/1.3238367.

Zhang, H., H. Liu, L. Liu, W. Jin, and X. Shi, 2014, Frequency domain acoustic equation high-order modeling based on an average-derivative method (in Chinese): Chinese Journal of Geophysics, **57**, 1599–1611, doi: 10.6038/cjg20140523.

Zhang, H., B. Zhang, B. Liu, H. Liu, and X. Shi, 2015, Frequency-space domain high-order modeling based on an average-derivative optimal method: 85th Annual International Meeting, SEG, Expanded Abstracts, 3749–3753.

Zhang, J.-H., and Z.-X. Yao, 2013, Optimized finite-difference operator for broadband seismic wave modeling: Geophysics, **78**, no. 1, A13–A18, doi: 10.1190/geo2012-0277.1.

Zhang, W., and Y. Shen, 2010, Unsplit complex frequency-shifted PML implementation using auxiliary differential equations for seismic wave modeling: Geophysics, **75**, no. 4, T141–T154, doi: 10.1190/1.3463431.